Fast Frequency Response from Offshore Wind Farms Connected to HVDC via Diode Rectifiers

Saborío-Romano, Oscar; Bidadfar, Ali; Sakamuri, Jayachandra Naidu; Göksu, Ömer; Cutululis, Nicolaos Antonio

Published in:
Proceedings of the Cigre Aalborg 2019: International Symposium

Publication date:
2019

Document Version
Publisher's PDF, also known as Version of record

Symposium Aalborg, Denmark
4th-7th June 2019

Paper Number: 42 (YM)

Fast Frequency Response from Offshore Wind Farms Connected to HVDC via Diode Rectifiers

O. SABORÍO-ROMANO*, A. BIDADFAR, J.N. SAKAMURI, Ö. GÖKSU, N.A. CUTULULIS

Department of Wind Energy
Technical University of Denmark
Risø Campus, Roskilde, Denmark

SUMMARY

Recently proposed as a viable alternative for connecting offshore wind farms (OWFs) to HVDC networks, diode rectifiers have prompted increasing interest from both industry and academia. However, before technical connection requirements for such solutions can be determined, more studies are needed to assess their capabilities to contribute to the secure operation of the networks connected to them.

This study assesses the capability of an OWF to provide frequency support to an onshore AC network, when connected through a HVDC link having a diode-rectifier-based (DR-based) offshore terminal and a voltage-source-converter-based (VSC-based) onshore terminal. The primary focus is fast frequency response (FFR), which contributes to the stabilisation of the onshore AC network during the first stage of large frequency excursions by decreasing the (magnitude of the) rate of change of frequency. The kinetic energy stored in the rotating masses of the wind turbines (WTs) is considered as the main source of additional power/energy for such response during onshore underfrequency events. The WTs are overloaded (i.e. forced to overproduce) to extract some of that stored kinetic energy when providing FFR during onshore underfrequency events. A semi-aggregated OWF representation is considered in order to examine the dynamics of each grid-forming wind turbine within a string when providing FFR, while achieving reasonable simulation times.

Simulation results corroborate that the new connection concept (and corresponding changes in WT control) does not have a significant impact on the capability of OWFs to provide FFR to onshore AC networks. That is OWFs connected to HVDC via DR-based offshore terminals can indeed provide FFR, by means of OWF-level active power controls similar to those developed for VSC-HVDC-connected OWFs, while its grid-forming WTs share the reactive power consumption/production and keep the offshore frequency and voltage within their normal operating ranges.

KEYWORDS

Diode-rectifier-based HVDC transmission – fast frequency response – frequency support – grid-forming wind turbine control – offshore wind energy integration – wind turbine overloading

*osro@dtu.dk

1 INTRODUCTION

Exploiting Europe's offshore wind resources fully will require more electrical infrastructure linking offshore wind farms (OWFs) and onshore networks. To date, most OWFs export their production via HVAC, and only a few are connected through HVDC [1]. The amount of HVDC-connected OWFs, however, is widely expected to increase, as the distance from shore and the size of OWFs increase, and the associated costs decrease [2], [3].

Since it was first introduced in 1997 [4], the HVDC transmission technology using voltage source (forced-/self-commutated) converters (VSCs), based on insulated-gate bipolar transistors, has experienced great development. Such HVDC transmission solutions still have higher losses and overall costs than the more common, mature ones employing (phase-controlled) line-commutated converters, based on thyristors (in a current source converter topology), which are largely used for bulk power transmission [3], [5]. However, VSC-based HVDC transmission (VSC-HVDC) offers advantages such as smaller footprints, fast reversibility of active power flow, independent control of active and reactive power, and the (grid-forming) capability to form AC networks, i.e. to control their AC-side voltage magnitude and frequency (allowing them to operate without the need of a strong AC grid) [4]. Due to of such advantages, the use of VSC-based offshore HVDC terminals has enabled the development of HVDC-connected OWFs with the prevailing grid-following approach to controlling wind turbines (WTs), in which WTs rely on other (grid-forming) units (e.g. offshore VSC-based offshore HVDC terminals) forming their AC network [1].

Recently proposed as a viable alternative for connecting OWFs to HVDC networks, (uncontrolled, line-commutated) diode rectifiers (DRs) have prompted increasing interest from both industry and academia [6]–[11]. DR-based offshore HVDC terminals offer advantages such as smaller footprints, higher efficiency, higher reliability and lower costs [8], [10]. However, as passive units, they lack the grid-forming capability of VSCs, so that their use relies on delegating such responsibility to the WTs. This requires fundamentally different WT and WF control schemes, changing their control approach from that of grid-following units to that of grid-forming units [6], [9].

For (grid-forming) WTs connected to HVDC via DR-based offshore terminals, providing frequency support (FS) to onshore AC networks must not interfere with their particular responsibility of keeping the offshore AC network's voltage (magnitude) and frequency within their operating ranges, as required by the use of such offshore terminals. To ensure optimal filter design and operation, their use also requires narrow operating frequency ranges (e.g. nominal frequency $\pm 0.25\,\%$ in steady state) in the offshore AC network. Owing to the nonlinear properties of DRs, their use requires a minimum OWF production limit (e.g. $2.5\,\%$) [12] as well, which can restrict the support that such OWFs can provide during onshore overfrequency events at low wind speeds.

The capability of VSC-HVDC-connected OWFs to provide FS to onshore AC networks has been investigated in [13]–[15] for two (point-to-point), three and four terminal HVDC networks, respectively. Moreover, current technical connection requirements for HVDC-interconnected offshore generation are based on the same paradigm of grid-forming controllable offshore HVDC terminals [16], [17]. Such requirements need to be adapted so as to include the possibility of having uncontrollable offshore HVDC terminals, if OWF connection concepts such as DRs are to be deployed. However, before specific requirements can be determined, more studies are needed to assess the capabilities of such solutions to contribute to the secure operation of the networks connected to them [12], [18].

The present study assesses the capability of an OWF to provide FS to an onshore AC network, when connected through an HVDC link having a DR-based offshore terminal and a VSC-based onshore terminal. The primary focus is fast frequency response (FFR), which contributes to the stabilisation of the onshore AC network during the first stage of large frequency excursions [19], [20]. The study also examines the compatibility of corresponding higher-level controls previously devised for VSC-HVDC-connected OWFs [13], [14]. Through such controls, the OWF modifies its active power output according to the

onshore frequency signal directly communicated to it. The kinetic energy stored in the rotating masses of the WTs has been considered as the main source of additional power/energy for such response during onshore underfrequency events. The WTs are overloaded (i.e. forced to overproduce) to extract some of that stored kinetic energy when providing FFR during onshore underfrequency events [19].

Previous work [21], [22] was conducted using models and grid-forming WT front-end converter (FEC) controls based on those in [6]–[8] and a single-machine aggregated representation of the OWF. Such controls rely on communication for a centralised control of the offshore AC network voltage and do not deal with the synchronisation of the WT FECs, whereas the aggregated OWF model does not provide enough insight into the dynamics within the OWF. This study uses more detailed models based on those in [19], and a semi-aggregated representation of the OWF. Such OWF representation provides insight into the dynamics of the WTs within a string by representing them in detail, while keeping reasonable simulation times. Moreover, the considered grid-forming WT FEC controls are based on those in [11], which rely solely on local measurements and enable the synchronisation of the WT FECs by means of a distributed phase-locked-loop-based frequency control algorithm.

The rest of the paper is organised as follows. In Section 2, the investigated system is described and the main control algorithm is detailed. In Section 3, some of the considered cases are described, and corresponding simulation results are presented and discussed. Finally, concluding remarks are made in Section 4.

2 MODELLING AND CONTROL

Figure 1 shows an overview of the studied system. The system is based on that described in [12], [19] and consists of a 400 MW OWF connected to an onshore AC network by means of a monopolar HVDC link. Balanced/symmetric operation is assumed. A lumped three-phase synchronous machine (SM) with its governor and turbine, and a lumped three-phase load represent the onshore AC network. The wind power share is 25 % (i.e. the OWF is rated at 400 MW, in a 1600 MW system). The onshore HVDC terminal consists of a VSC, which controls the voltage on its DC terminals and the reactive power injected into the onshore AC network. The offshore HVDC terminal, labelled in Figure 1 as *DR Platform*, consists of two (uncontrolled, line-commutated) diode-based 12-pulse rectifiers (DRs) connected in series, with corresponding reactive power compensation and filter bank on their AC side.

The OWF has 50 type-4 (full-converter) 8 MW WTs, laid out in 6 strings. The first string is comprised of WTs 1–9, which are represented in detail. The second string, consisting of WTs 10–18, is aggregated into an equivalent 72 MW WT and corresponding cable equivalent π circuit using the method proposed in

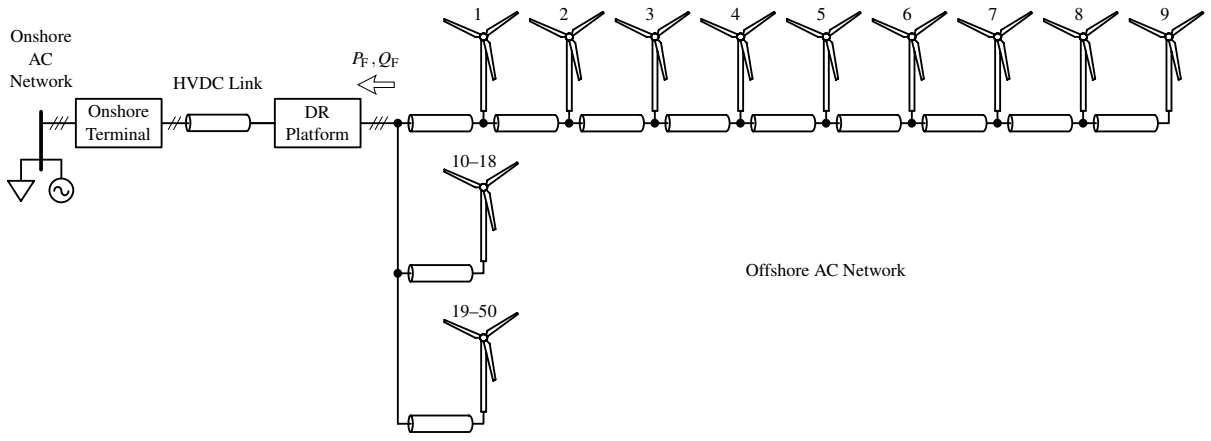

Figure 1: Overview of the studied system

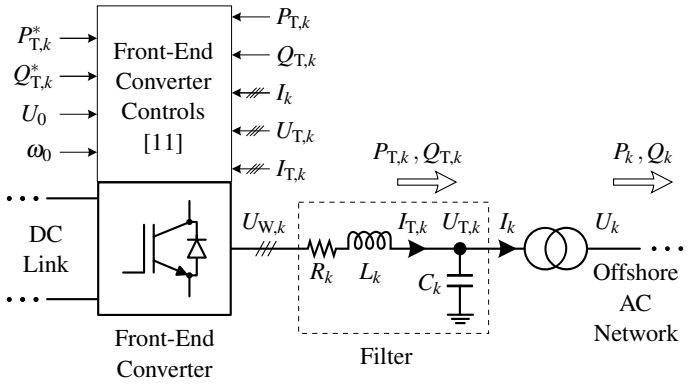

Figure 2: kth wind turbine front-end (line-side) network

[23]. Likewise, the other 4 strings, comprising WTs 19–50, are aggregated into an equivalent 256 MW WT and corresponding cable equivalent π circuit.

For computational efficiency, dynamics in the WT DC link and behind it are not considered, and the corresponding direct voltage is thus assumed constant (ideally regulated by the back-end/machine-side converter). Pulse-width modulation (PWM) is assumed to be done in the linear range, switching effects and any delay due to implementation of the PWM are neglected, and average value models are used to represent all VSCs. Focus is given to dynamics not faster than the VSC (inner/lower) current control loops, the fastest of which are designed to have a bandwidth of 200 Hz.

2.1 Wind Turbine Front-End Converter Controls

The front-end (line-side) network of the kth wind turbine(s), WT_k, is shown in Figure 2. The WT FEC controls are based on those proposed in [11] and are implemented on a rotating reference frame oriented on the voltage at the filter capacitor, $U_{\mathrm{T},k}$.

In each WT front-end network, the filter capacitor voltage direct (d) and quadrature (q) axis components, $U_{\mathrm{Td},k}$ and $U_{\mathrm{Tq},k}$, respectively, are regulated by the FEC lower/inner cascaded current and voltage control loops to follow the corresponding references while keeping the FEC output current, $I_{\mathrm{T},k}$, within its limits. The reference for $U_{\mathrm{Td},k}$ consists of two components: the offshore AC network voltage set point, U_0, common to all WTs, and a component individual to each WT, which is altered to control the FEC active power output, $P_{\mathrm{T},k}$. In an additional control loop based on the FEC phase-locked loop (PLL), a proportional controller manipulates the reference for $U_{\mathrm{Tq},k}$ to regulate the offshore AC network frequency, ω. The reference to such additional loop also consists of two components: the offshore AC network frequency set point, ω_0, common to all WTs, and a component individual to each WT, which is altered to control the FEC reactive power output, $Q_{\mathrm{T},k}$. When the WF is exporting power, the FEC upper/outer control loops in each WT regulate $P_{\mathrm{T},k}$ and $Q_{\mathrm{T},k}$ as follows. A proportional-integral (PI) controller regulates $P_{\mathrm{T},k}$ to follow the corresponding reference, $P^*_{\mathrm{T},k}$, whereas $Q_{\mathrm{T},k}$ is controlled by a proportional regulator (reactive-power-frequency droop) with a given reference, $Q^*_{\mathrm{T},k}$, so that reactive power is shared among WT FECs (avoiding overcurrents and reactive current circulation).

2.2 Wind Farm Active Power Control

To study the capability of such a WF to provide FS to an onshore AC network, the model is extended to include the supervisory active power control at plant level shown in Figure 3, based on those proposed in [13], [14] for OWFs connected to HVDC via VSCs. In the right side of Figure 3, a PI regulator controls the WF active power output, P_{F}, by altering the WF active power dispatch, P^*. A first-order low-pass filter (LPF) is applied to the corresponding measurement signal. Hardware and control limits are modelled by

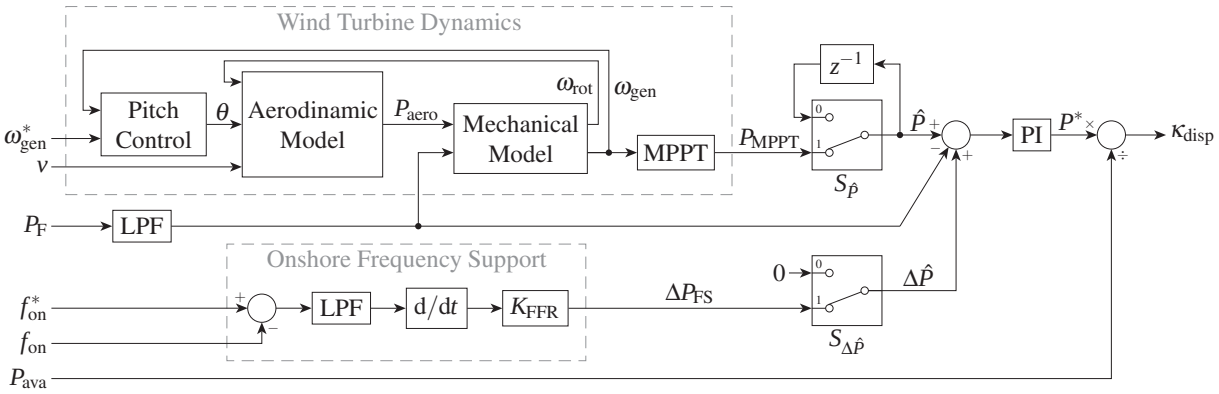

Figure 3: Wind farm active power control

means of corresponding restrictions on the regulator's output value and its rate of change. Proportional WF generation dispatch is used. In doing so, P^* is divided by the overall aerodynamic power available from the wind, P_{ava}, to generate the OWF active power dispatch coefficient, κ_{disp}. The active power set point of each WT FEC is then set as the product of the corresponding aerodynamic power available from the wind, $P_{ava,k}$, and the active power dispatch coefficient, i.e. $P^*_{T,k} = \kappa_{disp} P_{ava,k}$.

An internal aggregated model, shown in the top-left area of Figure 3, is included to take into account the WT dynamics relevant to WF active power modulation and WT overloading. It is based on those used in [14], [24] and consists mainly of an aerodynamic model, a mechanical model, a pitch control model and a maximum power point tracking (MPPT) look-up table.

In normal operation, the WT output power is controlled to follow the corresponding MPPT curve, $\hat{P} = P_{MPPT}(\omega_{gen})$, $\Delta\hat{P} = 0$, and is thus a function of the WT generator rotational speed, ω_{gen}. While operating on such curve, the WT aerodynamic efficiency is optimal for wind speeds lower than the nominal one, $v < 1\,\text{pu}$, the pitch control is inactive and the WTs operate at a constant zero pitch angle, $\theta = 0$. For higher wind speeds, the WTs run at rated power, and the pitch controller keeps ω_{gen} at its nominal value, i.e. $\hat{P} = P_{MPPT}(\omega_{gen} = \omega^*_{gen} = 1\,\text{pu}) = 1\,\text{pu}$, by manipulating θ (i.e. pitching the WT blades) so as to limit the aerodynamic/mechanical power extracted from the wind [24], P_{aero}.

2.2.1 Onshore Frequency Support and Wind Turbine Overloading

To provide FS to the onshore AC network, the base active power reference, $\hat{P}$, is modified, as shown at the bottom of Figure 3, by means of an additional active power reference, ΔP_{FS}, based on the onshore frequency, f_{on}, i.e. $\Delta\hat{P} = \Delta P_{FS}(f_{on})$. f_{on} is calculated from the alternating voltage measured at the onshore HVDC terminal's point of connection with the onshore AC network and is communicated continuously to the OWF with a delay of 100 ms. FFR is implemented by making ΔP_{FS} proportional to the rate of change of the deviation in f_{on} (to which a first-order LPF is first applied) from its nominal/reference value, $f^*_{on} = 1\,\text{pu}$.

When providing FFR during onshore underfrequency events, the WTs are overloaded to extract kinetic energy from their rotating masses. Two WT overloading methods are used, based on two different approaches to setting $\hat{P}$ during overloading: taking or not taking into account the resulting deceleration of the WT rotating masses. Such methods can be better understood by considering the WT dynamics depicted in Figure 4. The overloading period, T_{OL}, begins when the WTs start increasing their active power output in response to the onshore underfrequency event. During, T_{OL}, the power imbalance, $P_{aero} < P_F$, causes the WT rotating masses to decelerate (i.e. ω_{gen} decreases), which results in P_{MPPT} also decreasing. When the overloading is released, T_{OL} ends and the recovery period, T_{rec}, begins. During T_{rec}, $\Delta\hat{P} = 0$ and the WT rotating masses are allowed to recover their speed (i.e. ω_{gen} increases) by operating on the MPPT

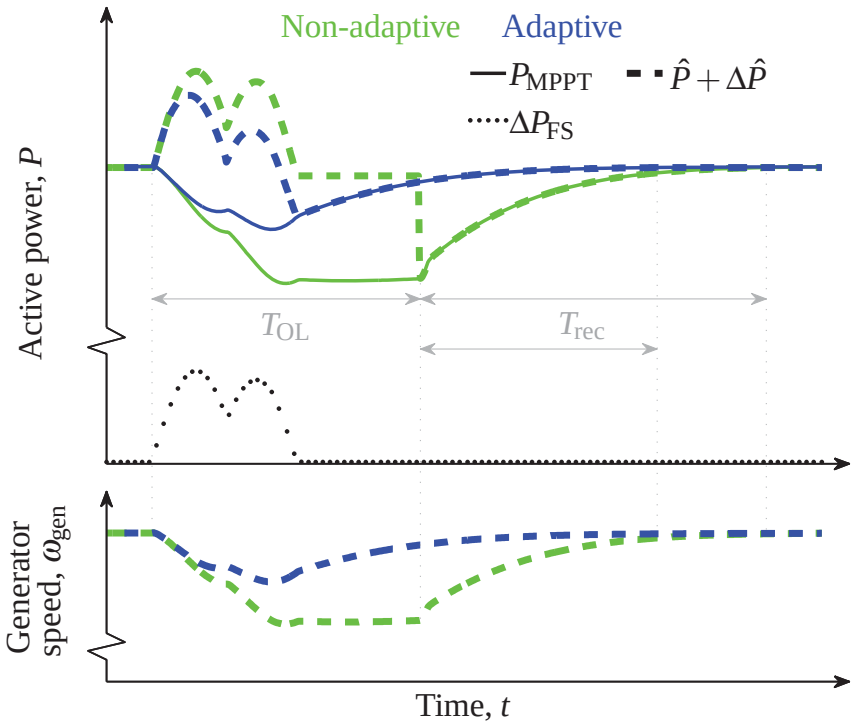

Figure 4: Wind turbine overloading methods

curve, $\hat{P} = P_{MPPT} \leq P_{aero}$, until $\hat{P} = P_{MPPT} = P_{aero}$.

In the non-adaptive overloading method, $\hat{P}$ is fixed at the (frozen) value of P_{MPPT} just before the start of T_{OL}, $\hat{P} = P_{MPPT_0}$. In the adaptive overloading method, the deceleration of the WT rotating masses during T_{OL} is taken into account by having $\hat{P} = P_{MPPT}(\omega_{gen})$. This allows the WT rotating masses to start recovering (once ΔP_{FS} goes back to zero) during T_{OL} and results in a lesser drop in the active power output and a shorter T_{rec} [14], [25].

3 SIMULATION RESULTS

Results of the dynamic simulations performed in PSCAD are presented in Figures 5 and 6, corresponding to onshore underfrequency events. The results depicted in Figure 5 correspond to the high wind speed scenario, whereas those illustrated in Figure 6 correspond to the medium and low wind scenarios. Table I details the wind speed scenarios considered in the simulations, in which P_{ava} denotes the overall aerodynamic power available from the wind. Wind speed (and the aerodynamic power available from it) is considered constant in each simulation. The considered individual WT operating points in Table I take into account the wind speed deficit due to the aerodynamic interaction between WTs. In principle, $P_{ava,k}$ decreases along the string in the wind speed direction [26]. All FEC controls have the same parameter (per-unit) values. Moreover, $U_0 = 0.86\,\text{pu}$, $\omega_0 = 1\,\text{pu}$ and $Q^*_{T,k} = 0$ for all of them.

Onshore frequency events are simulated by means of a 0.15 pu load step change (i.e. 240 MW/1600 MW)

Table I: Wind speed scenarios considered in the simulations

Wind	**Aerodynamic power available from the wind** [pu]											
Speed	P_{ava}	$P_{ava,1}$	$P_{ava,2}$	$P_{ava,3}$	$P_{ava,4}$	$P_{ava,5}$	$P_{ava,6}$	$P_{ava,7}$	$P_{ava,8}$	$P_{ava,9}$	$P_{ava,10-18}$	$P_{ava,19-50}$
Low	0.400	0.930	0.345	0.421	0.366	0.344	0.318	0.299	0.289	0.289	0.400	0.400
Medium	0.600	0.987	0.564	0.644	0.586	0.562	0.535	0.515	0.504	0.504	0.600	0.600
High	1.000	1.000	1.000	1.000	1.000	1.000	1.000	1.000	1.000	1.000	1.000	1.000

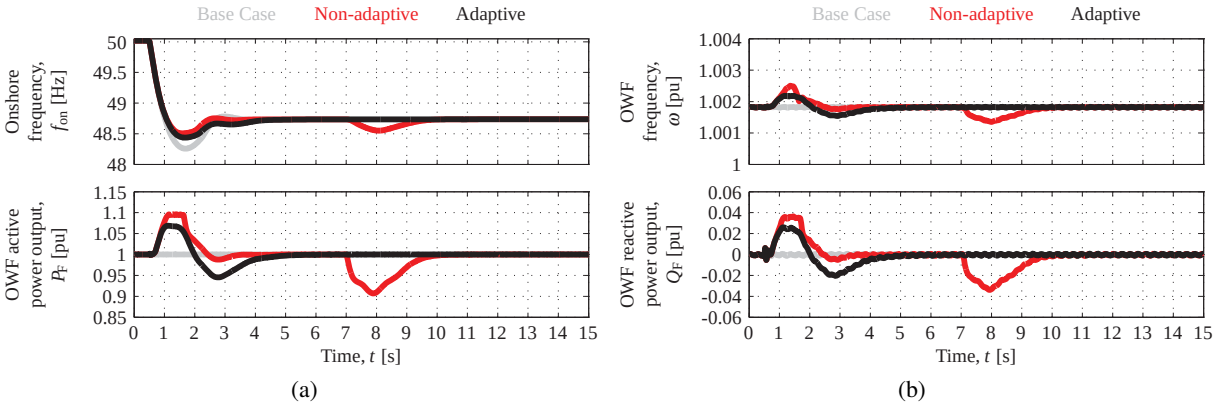

Figure 5: Wind farm response to an onshore underfrequency event at high wind speed

at $t = 0.5\,\text{s}$. Each figure includes base case responses, corresponding to no FS from the WF to the onshore AC network (i.e. the FS consisting solely of that of the SM). The (light) grey signals in each figure represent the base case, $\Delta\hat{P} = 0$, while the (dark) red and black traces illustrate the cases in which the WF provides FS, $\Delta\hat{P} = \Delta P_{\text{FS}}$. With regards to the WT overloading methods, the red and black curves depict the cases in which the non-adaptive method, $\hat{P} = P_{\text{MPPT}_0}$, and the adaptive method, $\hat{P} = P_{\text{MPPT}}$, are used, respectively. The overloading is released at $t = 7\,\text{s}$ (and not before) to accentuate the difference between the two methods. The onshore HVDC terminal keeps the HVDC link voltage close to the corresponding set point throughout all simulations.

The OWF response to an onshore underfrequency event at high wind speed is depicted in Figure 5. Similar results have been obtained for the other two wind speed scenarios. As can be seen in Figure 5a, the onshore frequency response can be improved by having the OWF provide FS to the onshore AC network. Once the OWF detects the underfrequency event, the frequency nadir is reduced by increasing P_{F} in proportion to the (magnitude of the) rate of change of frequency (ROCOF). The dip in P_{F} following the onshore frequency nadir reflects the change of sign of the ROCOF, used to generate the additional active power reference, $\Delta\hat{P} = \Delta P_{\text{FS}}$. When the overloading is released, P_{F} may decrease as the WTs recover their speed, producing a new frequency dip, as illustrated by the responses corresponding to the non-adaptive WT overloading method. If, however, the adaptive method is used for overloading the WTs, P_{F} follows (as depicted in Figure 4) the reduction in $P_{\text{MPPT}}(\omega_{\text{gen}})$ during the overloading period, T_{OL}. Such reduction in overproduction during T_{OL} results in a shorter recovery period (after releasing the overloading), with lesser reductions in P_{F} and f_{on}.

The changes in P_{F} result in proportional changes in the DR reactive power consumption. This is reflected in the changes in Q_{F} and ω in Figure 5b. However, such changes are one and three orders of magnitude smaller than that in P_{F}, respectively, while ω is kept close to 1 pu. That is the result of every grid-forming WT FEC contributing autonomously to regulating ω by means of its corresponding PLL-based (proportional) controller, while sharing the reactive power with the other grid-forming WT FECs by means of its reactive-power-frequency droop.

WT responses to an onshore underfrequency event at medium and low wind speeds are illustrated by Figures 6a and 6b, respectively. Solid and dashed traces—superimposed in the case of the WT terminal RMS voltages, U_k—represent the responses of WTs 1 and 9, respectively, corresponding to the turbines at both ends of the string that is represented in detail. Similar results have been obtained in the high wind speed scenario (in which $P_{\text{ava},k} = 1\,\text{pu}$ for all WTs). The WT active power outputs, P_k, reflect the assumed distributions of $P_{\text{ava},k}$ (Table I) and the changes in κ_{disp} when FS is provided.

In all wind speed scenarios, the changes in P_{F} in response to the onshore underfrequency event are achieved through changes in U_k which are two orders of magnitude smaller, keeping them within their

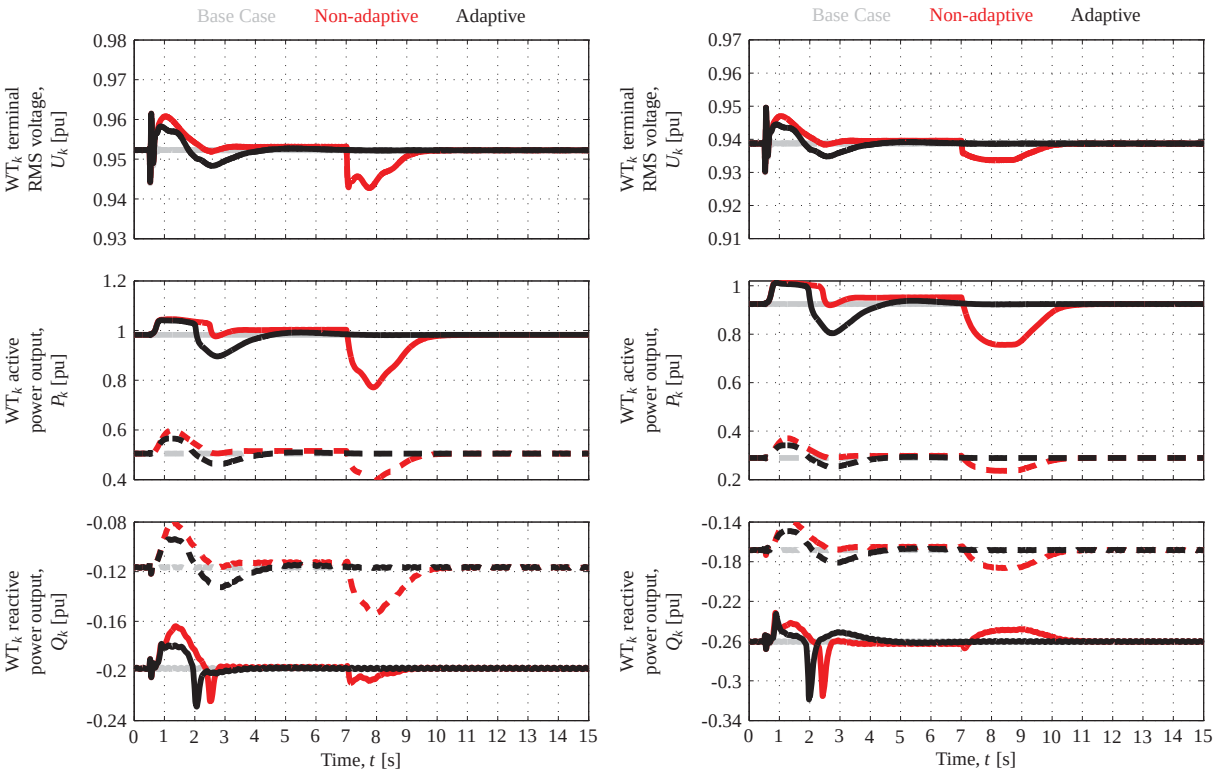

(a) Medium wind speed

(b) Low wind speed

Figure 6: kth wind turbine response to an onshore underfrequency event – Solid: $k = 1$, Dashed: $k = 9$

normal operating range, as depicted in both figures. As shown also in both figures, the WTs share the reactive power consumption (negative values of Q_k) according to their power rating and their active power output, P_k. Particular of the results corresponding to the medium and low wind speed scenarios are the responses of P_1 and Q_1 (i.e. the solid traces depicting the active and reactive power output of WT$_1$, respectively), in the middle and at the bottom, respectively, of Figures 6a and 6b. These are the result of the corresponding FEC limiting its output RMS current to 1.1 pu.

4 CONCLUSIONS

The simulation results indicate that the new connection concept (and corresponding changes in WT control) does not have a significant impact on the capability of OWFs to provide FFR by means of OWF-level active power control strategies similar to those developed for VSC-HVDC-connected OWFs. By overloading their WTs, the OWFs can provide more than the available aerodynamic power (overproduce) for several seconds during an onshore underfrequency event. This, nevertheless, can result in a new onshore frequency dip after the overloading is released. The use of an adaptive WT overloading method, which takes into account the resulting deceleration of the rotating masses, can help to reduce such adverse secondary effects. Employing such strategies, OWFs can provide FFR during onshore frequency events, reducing the frequency nadir/zenith, while their grid-forming WTs share the reactive power consumption/production and keep the offshore frequency and voltage within their normal operating ranges. The semi-aggregated OWF representation makes it possible to corroborate that for each grid-forming WT within the string represented in detail, while achieving reasonable simulation times. The reductions in the frequency nadir/zenith will, however, be limited by the delay in the communication of the onshore frequency signal and the constraints imposed on the value and rate of change of the OWF active power output.

5 ACKNOWLEDGEMENT

The authors gratefully acknowledge the contributions of Poul E. Sørensen to the discussions leading up to this work. This work has received funding from the European Union's Horizon 2020 research and innovation programme under grant agreement No 691714.

BIBLIOGRAPHY

[1] CIGRÉ Working Group B4.55, "HVDC Connection of Offshore wind power plant", Paris, France, Technical Brochure 619, May 2015.

[2] P. Bresesti, W. L. Kling, R. L. Hendriks, and R. Vailati, "HVDC Connection of Offshore Wind Farms to the Transmission System", *IEEE Transactions on Energy Conversion*, vol. 22, no. 1, pp. 37–43, Feb. 2007.

[3] D. van Hertem, O. Gomis-Bellmunt, and J. Liang, Eds., HVDC Grids: For Offshore and Supergrid of the Future. Hoboken, NJ, United States: John Wiley & Sons, Mar. 2016.

[4] ABB, "HVDC Light: It's time to connect", Tech. Rep., Mar. 2013. [Online]. Available: http://new.abb.com/docs/default-source/ewea-doc/hvdc-light.pdf.

[5] CIGRÉ Working Group B4.37, "VSC Transmission", Paris, France, Technical Brochure 269, Apr. 2005.

[6] R. M. Blasco-Giménez, S. C. Añó-Villalba, J. Rodríguez-D'Derlée, F. Morant-Anglada, and S. I. Bernal-Pérez, "Distributed Voltage and Frequency Control of Offshore Wind Farms Connected With a Diode-Based HVdc Link", *IEEE Transactions on Power Electronics*, vol. 25, no. 12, pp. 3095–3105, Dec. 2010.

[7] R. M. Blasco-Giménez, S. C. Añó-Villalba, J. Rodríguez-D'Derlée, S. I. Bernal-Pérez, and F. Morant-Anglada, "Diode-Based HVdc Link for the Connection of Large Offshore Wind Farms", *IEEE Transactions on Energy Conversion*, vol. 26, no. 2, pp. 615–626, Mar. 2011.

[8] S. I. Bernal-Pérez, S. C. Añó-Villalba, R. M. Blasco-Giménez, and J. Rodríguez-D'Derlée, "Efficiency and Fault Ride-Through Performance of a Diode-Rectifier- and VSC-Inverter-Based HVDC Link for Offshore Wind Farms", *IEEE Transactions on Industrial Electronics*, vol. 60, no. 6, pp. 2401–2409, Jun. 2013.

[9] T. Christ, S. Seman, and R. Zurowski, "Investigation of DC Converter Nonlinear Interaction with Offshore Wind Power Park System", in *Proceedings of the 2015 EWEA Offshore Conference*, Copenhagen, Denmark, 10th–12th Mar. 2015.

[10] P. Menke, R. Zurowski, T. Christ, S. Seman, G. Giering, T. Hammer, W. Zink, F. Hacker, D. Imamovic, J. Thisted, P. Brogan, and N. Goldenbaum, "2nd Generation DC Grid Access for Large Scale Offshore Wind Farms", in *Proceedings of the 14th Wind Integration Workshop*, Brussels, Belgium, 20th–22nd Oct. 2015.

[11] L. Yu, R. Li, and L. Xu, "Distributed PLL-Based Control of Offshore Wind Turbines Connected With Diode-Rectifier-Based HVDC Systems", *IEEE Transactions on Power Delivery*, vol. 33, no. 3, pp. 1328–1336, Jun. 2018.

[12] PROMOTioN, "Deliverable 3.1: Detailed functional requirements to WPPs", Project Deliverable, Dec. 2016. [Online]. Available: https://www.promotion-offshore.net/fileadmin/PDFs/D3.1_PROMOTioN_Deliverable_3.1_Detailed_functional_requirements_to_WPPs.pdf.

[13] L. Zeni, "Power system integration of VSC-HVDC connected wind power plants: Control principles, power system services, clustering of wind power plants", PhD thesis, Technical University of Denmark, Roskilde, Denmark, Mar. 2015.

[14] J. N. Sakamuri, "Coordinated control of wind power plants in offshore HVDC grids", PhD thesis, Technical University of Denmark, Roskilde, Denmark, Mar. 2017.

[15] A. Bidadfar, O. Saborío-Romano, M. Altin, N. A. Cutululis, P. E. Sørensen, E. Prieto-Araujo, and O. Gomis-Bellmunt, "Frequency Support Provision to Power Systems via HVDC-Based Offshore Wind Power Plants", in *Proceedings of the 17th Wind Integration Workshop*, Stockholm, Sweden, 17th–19th Oct. 2018.

[16] ENTSO-E, "Network Code on HVDC Connections (HVDC)", Brussels, Belgium, Network Code, Oct. 2015. [Online]. Available: https://www.entsoe.eu/major-projects/network-code-development/high-voltage-direct-current/Pages/default.aspx.

[17] ——, "Network Code on Requirements for Grid Connection Applicable to all Generators (RfG)", Brussels, Belgium, Network Code, Apr. 2016. [Online]. Available: https://www.entsoe.eu/major-projects/network-code-development/requirements-for-generators/Pages/default.aspx.

[18] O. Saborío-Romano, A. Bidadfar, Ö. Göksu, M. Altin, N. A. Cutululis, and P. E. Sørensen, "Connection of OWPPs to HVDC networks using VSCs and Diode Rectifiers: An Overview", in *Proceedings of the 15th Wind Integration Workshop*, Vienna, Austria, 15th–17th Nov. 2016.

[19] PROMOTioN, "Deliverable 3.2: Specifications of the control strategies and the simulation test cases", Project Deliverable, Mar. 2017. [Online]. Available: https://www.promotion-offshore.net/fileadmin/PDFs/D3.2_Specifications_Control_strategies_and_simulation_test_cases.pdf.

[20] R. Eriksson, N. Modig, and K. Elkington, "Synthetic inertia versus fast frequency response: A definition", *IET Renewable Power Generation*, vol. 12, no. 5, pp. 507–514, Apr. 2018.

[21] O. Saborío-Romano, A. Bidadfar, Ö. Göksu, and N. A. Cutululis, "Frequency Support from OWPPs connected to HVDC via Diode Rectifiers", in *Proceedings of the 16th Wind Integration Workshop*, Berlin, Germany, 25th–27th Oct. 2017.

[22] PROMOTioN, "Deliverable 3.5: Performance of ancillary services provision from WFs connected to DR-HVDC", Project Deliverable, Jan. 2018. [Online]. Available: https://www.promotion-offshore.net/fileadmin/PDFs/D3.5_PROMOTioN_Performance_of_ancillary_services_provision_from_WFs_connected_to_DR-HVDC.pdf.

[23] E. Muljadi, S. Pasupulati, A. Ellis, and D. Kosterov, "Method of Equivalencing for a Large Wind Power Plant with Multiple Turbine Representation", in *Proceedings of the IEEE PES 2008 General Meeting*, Pittsburgh, PA, United States, 20th–24th Jul. 2008.

[24] A. D. Hansen, M. Altin, I. D. Margaris, F. Iov, and G. C. Tarnowski, "Analysis of the short-term overproduction capability of variable speed wind turbines", *Renewable Energy*, vol. 68, no. 1, pp. 326–336, Aug. 2014.

[25] S. Wachtel, and A. Beekmann, "Contribution of Wind Energy Converters with Inertia Emulation to frequency control and frequency stability in power systems", in *Proceedings of the 8th Wind Integration Workshop*, Bremen, Germany, 14th–15th Oct. 2009.

[26] T. Göçmen, P. van der Laan, P. E. Réthoré, A. Peña-Díaz, G. C. Larsen, and S. Ott, "Wind turbine wake models developed at the technical university of Denmark: A review", *Renewable and Sustainable Energy Reviews*, vol. 60, pp. 752–769, Jul. 2016.